## Elucidating the Kinetic and Thermodynamic Driving Forces in Polymer Blend Film Self-Stratification

Samantha J. Rinehart<sup>1</sup>, Guangcui Yuan<sup>2,3</sup>, and Mark D. Dadmun\*,<sup>1,4</sup>

<sup>1</sup>Department of Chemistry, University of Tennessee, Knoxville, Tennessee 37996
<sup>2</sup>NIST Center for Neutron Research, National Institute of Standards and Technology, Gaithersburg, Maryland 20899

<sup>3</sup>University of Georgetown, Washington D.C. 20057 <sup>4</sup>Chemical Sciences Division, Oak Ridge National Laboratory, Oak Ridge, Tennessee 37830

\*Corresponding Author Information: Mark D. Dadmun, dad@utk.edu

#### Abstract:

Self-assembly of immiscible polymer blend films during deposition presents an attractive avenue to fabricate structured multi-component thin films. Depth profiles formed by self-stratification during spin casting can be varied simply by modifying processing conditions, even on short time scales. However, the current practice of self-stratification utilizes polymer blends that are specific for optimizing properties of a desired application and provides little insight into the underlying driving forces that guide the process of stratification. Our research seeks to fill this gap by using neutron reflectivity to monitor the stratification of blends consisting of poly(3-hexylthiophene-2,5-diyl (P3HT) and poly(methyl methacrylate) (PMMA) as a function of sample and processing condition: spin casting speed, polymer blend composition, and polymer molecular weight. Each of these parameters were varied individually, and each parameter provided orthogonal control of the extent of stratification. An increase in the concentration of P3HT in the blend composition increased the immiscibility between the two polymers which leads to an increase in stratification. A reduction in the similarity of polymer molecular weights in the blend reduced the entropic driving force of stratification. Additionally, when casting speed was decreased, and all thermodynamic conditions were left unchanged, we observed a longer film formation time and an increase in extent of stratification. Longer film formation times allow more time for the thermodynamic driving forces to dictate the rearrangement of polymer towards equilibrium. Furthermore, by changing the relative molecular weight of the polymers, the purity of the P3HT layer at the air interface improved, where the largest molecular weight PMMA resulted in the purest P3HT rich layer. The interfacial width between the P3HT rich layer

and the PMMA rich layer was also controlled by changing the composition of the blend, where the blend with the highest concentration of P3HT resulted in the sharpest interface. We attribute the differences in vertical morphology to the control of the thermodynamic properties of each blend, including total entropy of the system, surface energy, and the  $\chi$  interaction parameter. Through careful regulation of the processing conditions of P3HT:PMMA thin films, these results provide insight into *both* the kinetic and thermodynamic factors that direct the self-stratification of polymer blend films. This fundamental study of stratification for P3HT:PMMA blends provides the foundation to develop a global understanding of self-stratification and to impact a wide range of technologies by developing cost-efficient protocols for multi-layer film deposition of structured thin films without post-modification processes.

#### **Introduction:**

Polymer coatings serve a wide array of purposes, where many specific applications require multi component coatings.<sup>1–5</sup> These coatings are typically applied in a layer by layer fabrication process. In addition to the deposition of each layer for its desired application, adhesive binders are often required between layers to prevent peeling and improve durability of the entire coating system.<sup>1</sup> This layer by layer assembly is inefficient and in order to combat this, the stratification of multiple materials from a single step solution process may be employed to improve the efficiency of film fabrication.<sup>6–8</sup> Utilizing self-stratification decreases the number of depositions which leads to lower production costs as it eradicates time consuming post-modification processes of the material.<sup>9</sup>

Much of the current investigation of self-stratification of blend films involves altering the processing conditions and correlating these processing conditions to final film properties, for example device performance or durability.<sup>10–14</sup> To the best of our knowledge, there is limited knowledge of the thermodynamic and kinetic driving forces that guide the self-stratification process, which is needed to more rationally control of final film morphology.<sup>15</sup> For example, in many thin film applications, polymers processed from different casting solvents result in films with contrasting properties.<sup>16</sup> Yet it is unclear whether changing the solvent has a larger impact upon the kinetic drying time of the film, or the

thermodynamic interactions of the system, and which of these two properties controls and guides the formation processes that impact the final film structure and properties. Our studies will focus on the common film formation process of spin coating, which is a non-equilibrium process. <sup>17,18</sup> Therefore, in order to identify the driving forces that guide film formation, it is necessary to regulate multiple parameters to derive an understanding of the thermodynamic and kinetic processes that impact the measured film structure and properties.

Typically, stratification is examined via depth profiles derived from optical microscopy, or ion sputtering mass spectroscopy, <sup>19–21</sup> both of which provide a qualitative picture of the polymer blend stratification. Our research will utilize neutron reflectivity to provide a quantitative assessment of the impact of spin casting speed, polymer blend composition, and polymer molecular weight on the stratified sample's depth profile and structure. These processing parameters were selected to provide insight into the effect of surface energy, polymer-polymer interaction parameters, and film drying kinetics on final film formation and polymer blend stratification. To realize this goal, a quantitative method was developed to analyze the final film's extent of stratification, so that the thermodynamic and kinetic driving forces that guide final film structure and total stratification can be more thoroughly investigated.

The focus of this research is a conjugated and insulating polymer blend, poly(3-hexylthiophene-2,5-diyl) (P3HT) and poly(methyl methacrylate) (PMMA), which are used as benchmark polymers for organic field effect transistors. Utilizing these two polymers is advantageous because they phase separate upon deposition into practical morphologies suitable for solution processing of electronic devices. Recent studies have documented how specific deposition conditions impact the performance of these devices, but disregard how the thin film structure and thus, in turn, device performance may be *tuned* with control of the final blend film stratification. Providing insight into the role of specific thermodynamic and kinetic parameters on the film formation process will greatly impact the ability to control, engineer, and improve these films for desired application performance. Provides an innovative pathway to control final film morphology simply by changing the polymer blend and processing conditions.

#### **Experimental:**

Chlorobenzene (Sigma Aldrich), Poly(3-hexylthiophene-2,5-diyl) (P3HT) (Ossila, regioregularity-95%, and number-average molecular weight (M<sub>n</sub>) 19,500 g/mol and polydispersity index (PDI) 1.75) and deuterated poly(methyl methacrylate (dPMMA) (Polymer Source Inc., M<sub>n</sub> (PDI), 20,000 g/mol (1.6), 131,500 g/mol (1.4), 316,000 g/mol (1.35), 520,000 g/mol (1.4)) were used directly from the supplier and were not further purified. Polymer blends were dissolved at 1 percent by mass in ratios of P3HT:dPMMA 5:95, 10:90, 15:85, 20:80 in chlorobenzene. These polymer blends were dissolved at 55 °C overnight into a homogenous solution. Thin films were prepared by spin coating (209.4 rad/s, 104.7 rad/s, and 52.4 rad/s) the chlorobenzene solutions onto Si wafers. The Si wafers were cleaned in a piranha solution (3:1 ratio of sulfuric acid and hydrogen peroxide), washed with nanopure water, and allowed to sit under UV irradiation and ozone for 30 minutes prior to film deposition.

Neutron reflectivity experiments were conducted at both the National Institute of Standards and Technology's Center for Neutron Research using the NG7 beamline and the Spallation Neutron Source at Oak Ridge National Laboratory with a Q range of 0.008-0.2 A<sup>-1</sup> where Q=  $4\pi/\lambda \sin(\theta)$ ;  $\lambda$  is the neutron wavelength, and  $\theta$  is the angle of incidence. The data for all incident angles was reduced utilizing the NCNR software.<sup>32</sup>

Time-resolved light reflectivity was measured with an in-situ apparatus to monitor film formation during the spin casting process under the same conditions discussed above. A P3HT:dPMMA (520,000 g/mol) 20:80 solution was spin cast at 209.4, 104.7, and 52.4 rad/s. The procedure is described elsewhere.<sup>18</sup>

The surface energy of protonated poly(methyl methacrylate) (H-PMMA) was determined using contact angle measurements. H-PMMA was obtained from Acros (M<sub>n</sub> 15,000 g/mol) and Sigma-Aldrich (weight average molecular weight (M<sub>w</sub>) 120,000 g/mol and 350,000 g/mol). M<sub>n</sub> 520,000 g/mol dPMMA was obtained from Polymer Source. Contact angle measurements were conducted at the Chemical Sciences Division at Oak Ridge National Laboratory utilizing a Kruss DSA 100 Standard Optical Microscope. Drops

of water and diiodomethane were placed on thin films of bare  $SiO_2$ , P3HT, and PMMA with  $M_n$  of 520,000 g/mol,  $M_w$  350,000 g/mol,  $M_w$  120,000 g/mol, and  $M_n$  15,000 g/mol in these experiments.

#### **Results:**

In order to study the impact of processing conditions on final film structure, the depth profile of the samples of interest were determined by neutron reflectivity experiments, where parameters of interest include polymer blend composition, spin casting speed, and PMMA molecular weight. Each experiment resulted in a raw neutron reflectivity curve which was fit to a multi-layer model using IGOR and Motofit software packages.<sup>33</sup> The model fit was verified for accuracy by incorporating a mass balance where the average scattering length density (SLD) for the model depth profile is compared to the average SLD of the polymer blend based on the composition of the spin cast solution within 3% agreement. The fitting procedure produces a depth profile of SLD as a function of thickness. Each SLD is then transformed into a P3HT volume fraction depth profile using Equation 1:

$$\frac{SLD_{layer}(z) - SLD_{dPMMA}}{SLD_{dPMMA} - SLD_{P3HT}} = \phi_{P3HT}(z)$$
 Eq. (1)

where  $SLD_{layer}(z)$  is the SLD of the model depth profile at depth z, and  $\phi_{P3HT}$  is the volume fraction of P3HT in the layer. The SLD of P3HT is estimated to be  $0.7 \times 10^{-6} \, \text{A}^{-2}$  and a range of  $6.7 \times 10^{-6} \, \text{A}^{-2} - 7.1 \times 10^{-6} \, \text{A}^{-2}$  was used for the range of molecular weights of dPMMA, calculated from the National Institute for Standards and Technology (NIST) Center for Neutron Research (NCNR) SLD calculator. The thickness of each sample was normalized using the measured thicknesses from the neutron fit, where 0 is the air interface and 1 is the SiO<sub>2</sub> interface. The normalized film thickness allows the comparison of all films regardless of processing conditions where film thickness is known to change with polymer molecular weight and spin casting speed.<sup>34</sup>

Each P3HT volume fraction depth profile was further analyzed to quantitatively determine the extent of stratification of each sample. In this analysis, the stratification is quantified by comparing the depth profile of the experimental film to that of a completely stratified sample and a homogenous thin film.

A completely stratified sample is defined as two layers of pure P3HT and pure dPMMA and a homogenous thin film is a film with a constant concentration of P3HT throughout the entire depth of the film.

We can compare the stratification of different samples regardless of processing conditions by utilizing a normalized thickness and the percent of P3HT in the samples as a baseline for each calculation. To determine the amount of P3HT in each sample, the total integral of the volume fraction depth profile (0% to 100% P3HT) as a function of normalized thickness (0 to 1) is determined. This integral value is then used as the baseline in the depth profile for the extent of stratification calculation, because a completely homogenous (i.e. non-stratified) film contains this amount of P3HT, regardless of the probed depth. Equation 2 provides the method to calculate the extent of stratification, *S*, of a polymer blend film.

$$S = 100 * \frac{V_{\text{sample}}}{(100 - V_{\text{total}}) * (\frac{V_{\text{total}}}{100})}$$
Eq. (2)

In Equation 2,  $V_{total}$  is the integral under a sample's depth profile curve (baseline 0% P3HT) which represents the volume percent of P3HT in the entire deposited film. The value obtained for  $V_{total}$  is used for the baseline of the integral denoted as  $V_{sample}$ . The value of the volume fraction of the P3HT in the film,  $V_{total}$ , is used as the baseline for  $V_{sample}$  ensuring that a homogenous, non-stratified sample is quantified as 0 percent stratified. Any area above the theoretical limit of a homogenous, non-stratified sample indicates stratification occurred. The integral denoted as  $V_{sample}$  represents a quantitative measure of the stratification of each sample.  $V_{sample}$  is the area under the depth profile of the experimental film with the average concentration of P3HT in the deposited film (that can be determined from  $V_{total}$ ) as the baseline. For further clarification, this method is illustrated in Figure 1 for a sample consisting of a blend of P3HT:dPMMA 20:80. The horizontal dashed line at 20% P3HT describes the baseline of the  $V_{sample}$  integral, as the P3HT volume fraction of this sample is 20%. The vertical line at 0.2 thickness of the film represents the hypothetical thickness of a P3HT layer in a completely stratified film consisting of 20% P3HT. To calculate the extent of stratification of the sample,  $V_{sample}$  is divided by the area of a completely stratified layer with the horizontal baseline of 20 (volume percent of P3HT in the film) and the vertical outlined rectangle in Figure

1. The area of the vertical rectangle above the horizontal baseline of  $V_{total}$  is calculated as the denominator in Equation 2 ((100-V<sub>total</sub>)•(V<sub>total</sub>/100)). The vertical and horizontal limits change in the calculation of S for each sample to account for changes in the P3HT composition in the film during the spin coating process. The extent of stratification for this sample is defined by the area under the depth profile curve and above the horizontal baseline (checkerboard pattern) (8), divided by the area of the outlined rectangle above the horizontal  $V_{total}$  baseline (100-20)•(20/100)=16); 8/16=50% stratified. The error for the extent of stratification is calculated from difference between the experimental volume percent of P3HT in the film (V<sub>total</sub>) and the theoretical P3HT concentration based on the spin cast solution. The discrepancy between the experimental and theoretical P3HT concentrations is propagated through Equation 2.

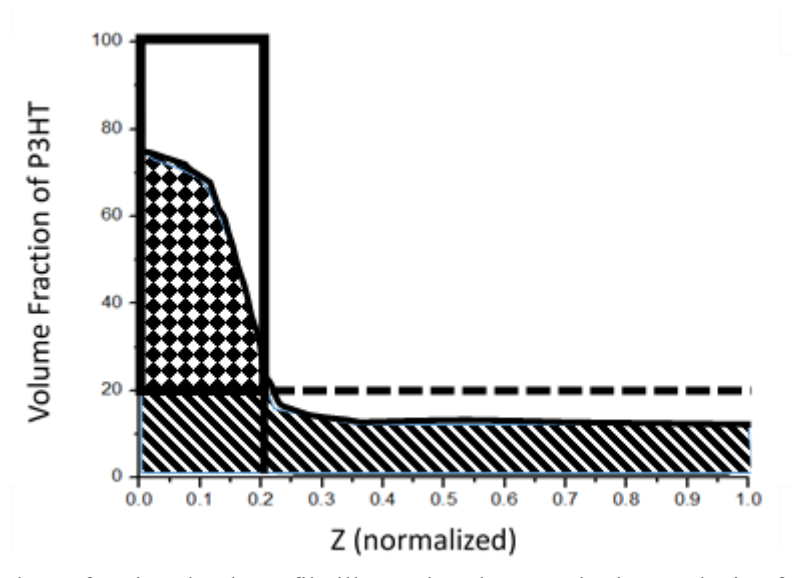


**Figure 1.** P3HT volume fraction depth profile illustrating the quantitative analysis of percent stratification, where  $V_{total}$  measures the sum of the areas of the black and white stripe region and the black and white checkerboard region,  $V_{sample}$  measures the area of the black and white checkerboard region, and the black horizontal baseline represents the baseline for  $V_{sample}$  which is equivalent to the concentration of P3HT in the sample.

Using this protocol, the extent of stratification of spin-coated P3HT:dPMMA polymer blends were monitored as a function of spin casting speed, P3HT:dPMMA blend composition and dPMMA molecular weight. First, the impact of P3HT:dPMMA blend composition will be reported. Figure 2 shows the resultant P3HT volume fraction depth profiles as a function of nominal blend composition. The compositions analyzed are P3HT:dPMMA blends of 5:95, 10:90, 15:85, 20:80. Altering the blend composition (Figure

2) clearly results in different degrees of P3HT found at the air interface, though all samples are stratified to some extent. As the P3HT concentration increases in these samples, the depth of the P3HT layer at the air interface broadens. In addition, the sharpness of the interface between an upper layer dominated by P3HT and the lower layer dominated by dPMMA varies for the blends. The breadth of the interface between these two layers is related in Figure 2 to the slope of the depth profile between layers, where a steep slope is interpreted to be a sharp interface while a gradual slope depicts a broad interface. The 5:95 P3HT:dPMMA sample has a broad interface that becomes sharper as the P3HT loading increases, with a significantly sharp interface observed in the 20:80 blend. Figure 3 plots the extent of stratification of the P3HT:131,500 g/mol dPMMA samples for all blend compositions. It is evident that an increase in P3HT loading increases the extent of stratification for each sample.

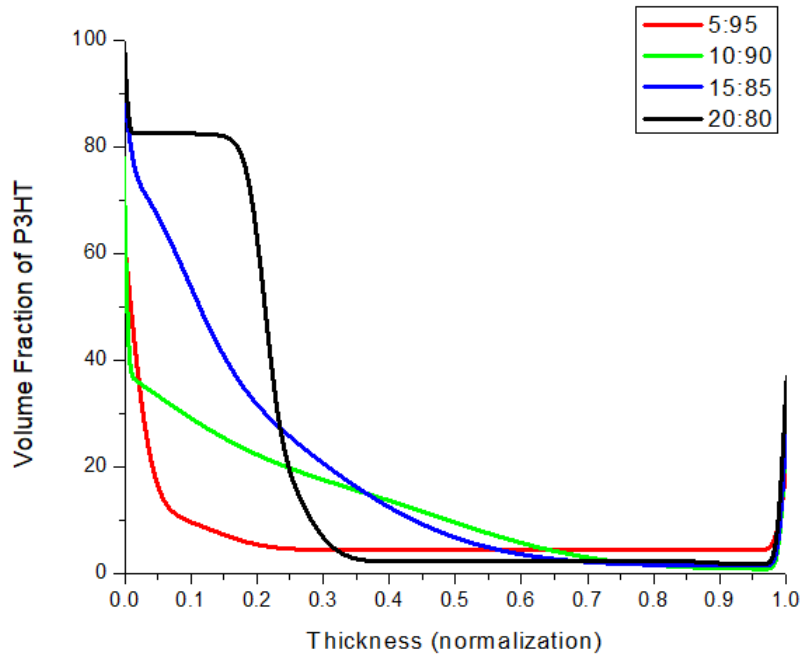


**Figure 2.** P3HT volume fraction depth profiles of P3HT:131,500 g/mol dPMMA 5:95 (red), 10:90 (green), 15:85 (blue), 20:80 (black) blends spin cast from chlorobenzene at 104.7 rad/s where 0 is the air interface and 1 is the SiO<sub>2</sub>.

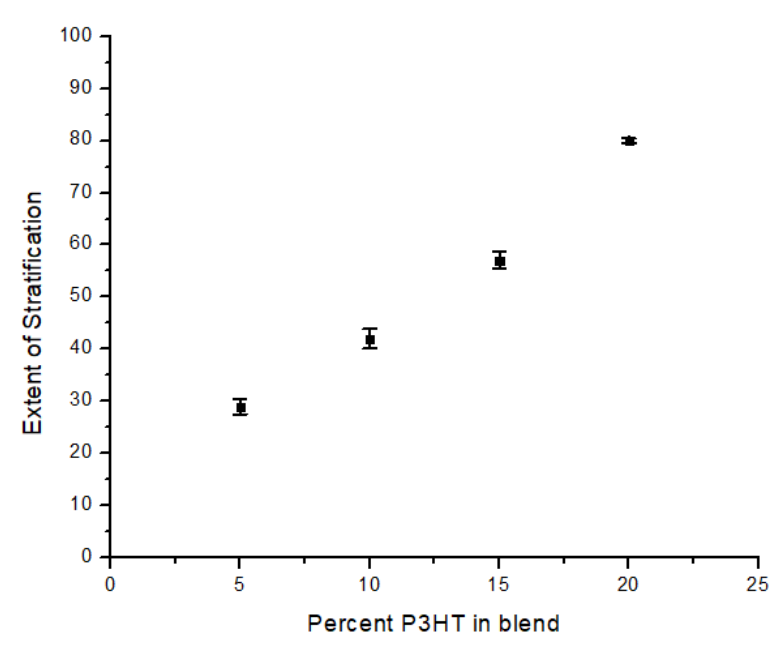


**Figure 3.** Plot of the extent of stratification as a function of P3HT loading all prepared at 104.7 rad/s and 131,500 g/mol dPMMA.

It has been previously reported that spin casting conditions directly impact film formation time.<sup>30</sup> One method to extend film formation time is to introduce a different spin casting solvent with a higher boiling point.<sup>35</sup> Changing the solvent allows us to investigate the effect of film formation time on the degree of stratification, but additional solvent-polymer interactions must be considered. As an attempt to isolate the effect of film formation time on the extent of stratification without introducing additional polymer-solvent interactions, the impact of spin-casting speed on film formation time, and thus, final film structure was monitored. To quantify the time required for film formation at each spin speed, time resolved light reflectivity experiments were conducted. Figure 4 presents the light reflectivity results for each spin speed (52.4, 104.7, 209.4 rad/s). Interpreting these results provides a film formation time when the constructive and destructive interference fridges no longer appear. This flat line is due to an increase in off specular scattering relative to the light reflectivity fringes in a dry film. These results show that P3HT:dPMMA blend solutions spun at 52.4 rad/s formed films in 21 seconds, solutions spun at 104.7 rad/s formed films in 11 seconds, and solutions spun at 209.4 rad/s formed films in 6 seconds.

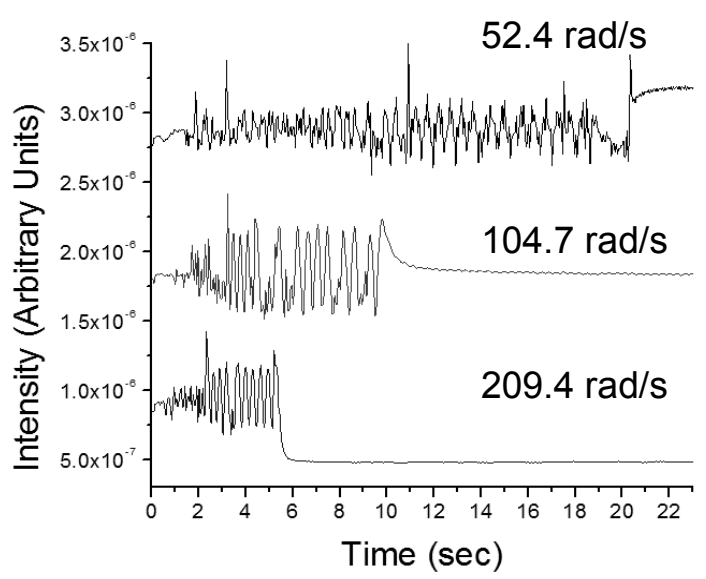


**Figure 4.** Light reflectivity monitoring film formation of a P3HT:dPMMA 20:80 blend spin cast at 52.4 rad/s (top), 104.7 rad/s (middle), and 209.4 rad/s (bottom).

The volume fraction depth profiles and extent of stratification for samples prepared with different casting speeds are reported in Figures 5 and 6, respectively. Figure 5 displays the P3HT volume fraction depth profile for the P3HT:dPMMA 20:80 blends containing 131,500 g/mol dPMMA as a function of spin cast speed. It is interesting to note that the sharpness of the interface between the P3HT dominated layer and dPMMA dominated layer does not change with spin cast speed. The change in spin cast speed, and therefore time of film formation, does alter the concentration of P3HT in the top layer, though it does not change the normalized thickness of this layer. In these samples, the 52.4 rad/s sample contains the highest concentration of P3HT in the top layer, while the 209.4 rad/s sample contains the smallest concentration of P3HT in the top layer. It is important to note that although this representation of the data does not show a broadening of the P3HT layer with spin speed, each sample's thickness has been normalized to 1. Therefore, the P3HT rich layer is thicker in the sample cast at 52.4 rad/s (~19 nm) than the sample cast at 209.4 rad/s (~4 nm), but this difference is minimalized when the total thickness of the film is normalized. The total thicknesses of the 52.4 rad/s and 209.4 rad/s films are ~65 nm and ~30 nm, respectively.

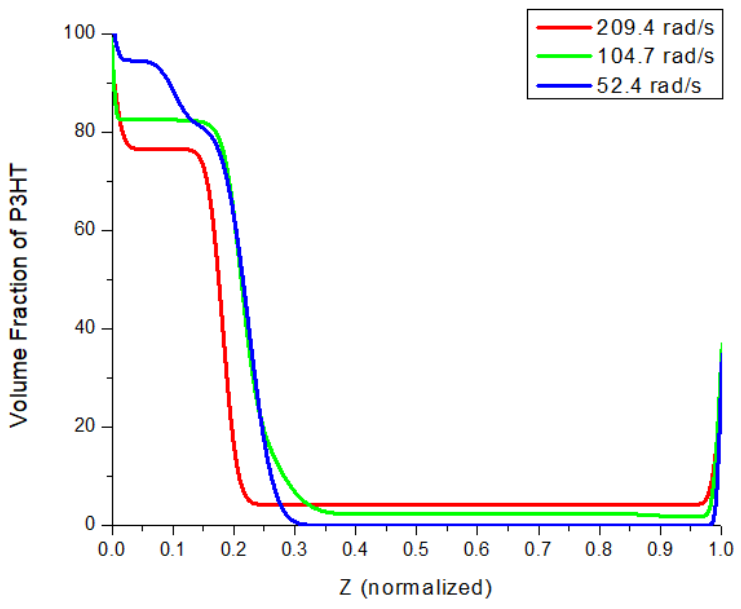


**Figure 5.** P3HT volume fraction depth profiles of a P3HT:dPMMA (131,500 g/mol) 20:80 blend spin cast from chlorobenzene at 209.4 rad/s (red), 104.7 rad/s (green), and 52.4 rad/s (blue) where 0 is the air interface and 1 is the SiO<sub>2</sub>. Repeats of P3HT:dPMMA (131,500 g/mol) 20:80 samples prepared at 104.7 rad/s and 209.4 rad/s are included in the supplementary information.

To quantify the exact changes of the stratification with the change in processing conditions, the P3HT volume fractions were analyzed to quantify the extent of stratification with the method described by Equation 2. Figure 6 shows the extent of stratification as a function of the composition of the P3HT:dPMMA blend as well as the spin-casting speed for each thin film. Figure 6 also shows that at each specific spin speed, an increase in P3HT loading results in a larger percent stratification. In addition, Figure 6 also shows that for each P3HT:dPMMA composition, a spin speed of 52.4 rad/s results in the largest extent of stratification. Qualitatively, the stratification of the final film increases with decreasing spin speed and increasing film formation time.

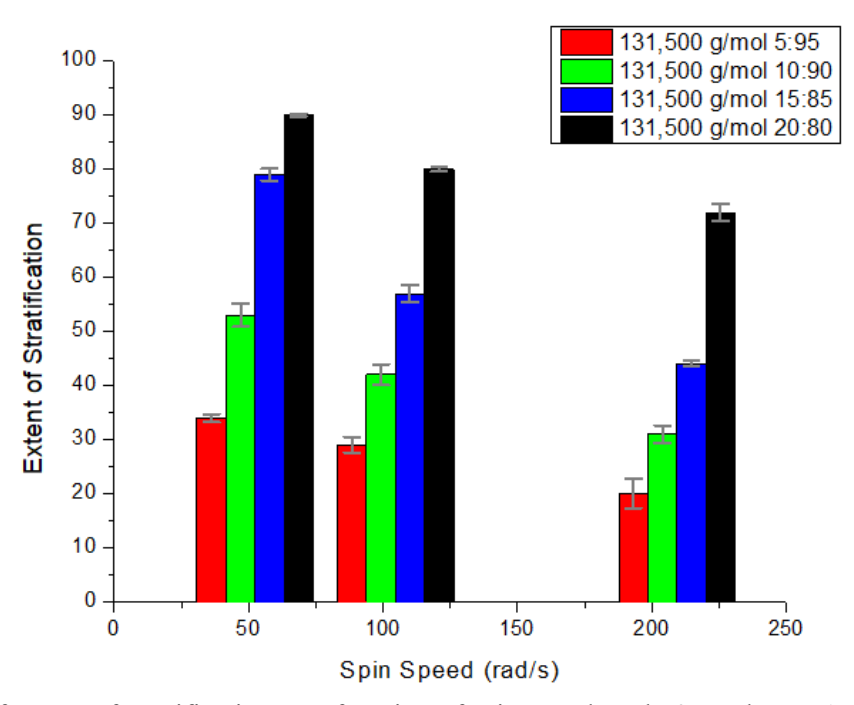


**Figure 6.** Plot of extent of stratification as a function of spin speed, and P3HT:dPMMA composition 5:95 (red), 10:90 (green), 15:85 (blue), 20:80 (black). The P3HT volume fraction profiles for P3HT:dPMMA 131,500 g/mol samples of all blend compositions prepared at casting speeds of 52.4 and 209.4 rad/s can be found in the supplementary information. Additionally, repeats of P3HT:dPMMA (131,500 g/mol) 5:95 samples prepared at 52.4 rad/s and 104.7 rad/s are included in the supplementary information.

The molecular weight of dPMMA was also varied to observe its effect on the P3HT stratification process. For this set of experiments, four different dPMMA molecular weights were employed (20,000 g/mol, 131,500 g/mol, 316,000 g/mol, and 520,000 g/mol). Films were formed from solutions with P3HT:dPMMA compositions of 5:95, 10:90, 15:85, 20:80, where solutions were spin cast at 104.7 rad/s from chlorobenzene. Figure 7 shows the P3HT volume fraction depth profiles for the 5:95 P3HT:dPMMA blends for each molecular weight.

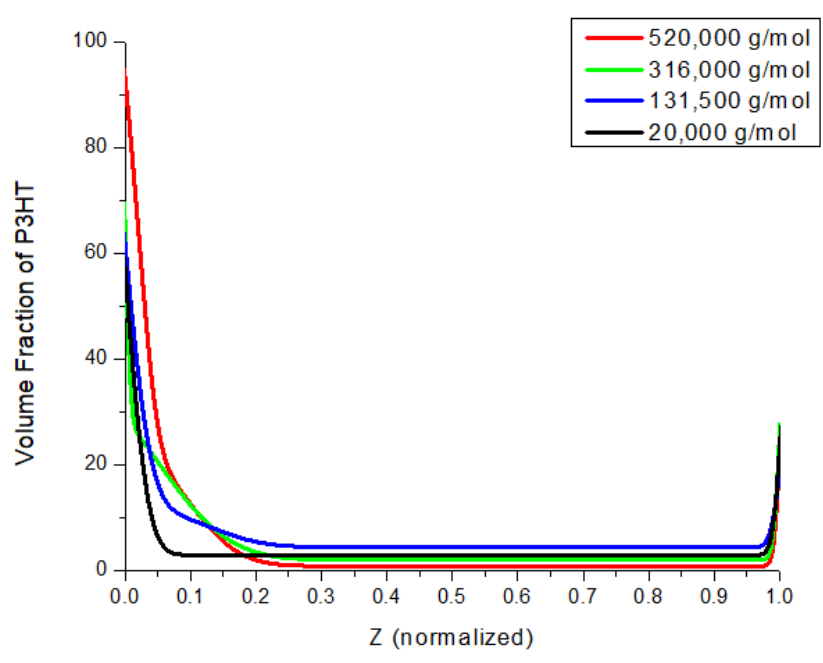


**Figure 7.** P3HT volume fraction depth profiles of a P3HT:dPMMA 5:95 blend spin cast from chlorobenzene at 104.7 rad/s with varying dPMMA molecular weights 520,000 g/mol (red), 316,000 g/mol (green), 131,500 g/mol (blue), 20,000 g/mol (black) where 0 is the air interface and 1 is the SiO<sub>2</sub> interface.

The film formed from the blend containing the largest molecular weight dPMMA 520,000 g/mol has a small layer of highly concentrated P3HT at the air surface, and as the molecular weight of dPMMA decreases, the P3HT concentration at the air interface decreases. The interface between the P3HT dominated region and the dPMMA dominated region does not seem to change significantly among the various molecular weight depth profiles. To quantify the effects of dPMMA molecular weight on stratification, each depth profile was analyzed using Equation 2, and the resultant extents of stratification are shown in Figure 8.

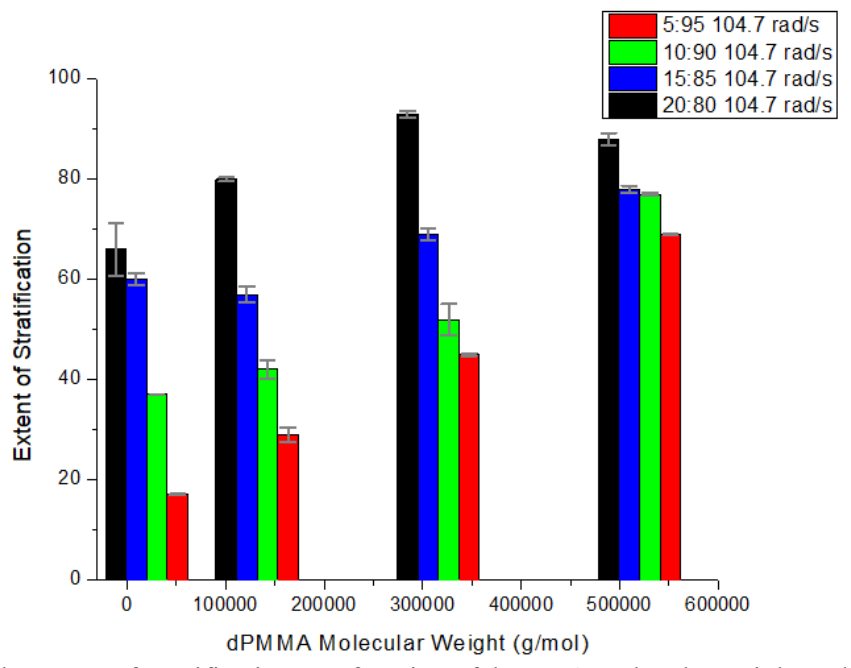


**Figure 8.** Plot of the extent of stratification as a function of dPMMA molecular weight and P3HT:dPMMA composition 5:95 (red), 10:90 (green), 15:85 (blue), 20:80 (black) all prepared at 104.7 rad/s. The P3HT volume fraction profiles for P3HT:dPMMA 20,000 g/mol, 316,000 g/mol, and 520,000 g/mol samples can be found in the supplementary information.

Inspection of Figure 8 shows that for each blend composition, the extent of stratification generally decreases as dPMMA molecular weight decreases. It is important to note that the change in extent of stratification with respect to blend composition in these experiments, where an increase in P3HT in the blend leads to an increase in stratification, agrees with the trends observed in the stratification patterns and extent of stratification values shown in Figures 2, 3, and 6. Additionally, the change in extent of stratification with blend composition is significantly reduced in the 520,000 g/mol dPMMA blend relative to the changes in the extent of stratification with blend composition for films that contain 20,000 g/mol dPMMA. The blends containing 520,000 g/mol dPMMA exhibit a variation in extent of stratification that is only *ca.* 15% with blend composition, while the extent of stratification in the 20,000 g/mol dPMMA blends varies from less than 10% to greater than 60% with changes in the blend composition.

To further investigate the driving forces behind stratification differences when varying dPMMA molecular weight, contact angle measurements were conducted using water and di-iodomethane to determine the surface energy of each molecular weight dPMMA, P3HT, and SiO<sub>2</sub>. The contact angle

measurements as well as their respective surface energies are presented in Table 1. Surface energy was calculated using the geometric mean method as shown in Equation 3:<sup>36</sup>

$$(1 + \cos \theta_t)\gamma_t = 2[(\gamma^d_t \gamma^d_s)^{1/2} + (\gamma_t^p \gamma_s^p)^{1/2}]$$
 Eq. (3)

In Equation 3,  $\theta$  is the contact angle of the test liquid on a solid surface, and  $\gamma_t$  and  $\gamma_s$  are the surface energies of the test liquid and the solid surface, respectively. The accepted polar (p) and dispersive energy (d) components for water are 51.0 mJ/m² and 21.8 mJ/m² and for diiodomethane are 0.0 mJ/m² and 50.8 mJ/m². The surface energy of PMMA increases with decreasing molecular weight, and the surface energy of PMMA is always larger than that of P3HT. P3HT and all molecular weights of PMMA have significantly different surface energies than that of the SiO<sub>2</sub> substrate. The decrease in the surface energy of dPMMA with molecular weight is accredited to an end group effect, where an increase in the number of chain ends in low molecular weight polymers relative to their high molecular weight counterparts alters the polymer surface energy.

**Table 1.** Contact angles and calculated surface energies and measurements of the polymers studied.

Sample	H <sub>2</sub> O Contact Angle (°)	CH <sub>2</sub> I <sub>2</sub> Contact Angle (°)	Surface Energy (mJ/m²)
15,000 g/mol PMMA	74.5	32.4	46.5
100,000 g/mol PMMA	73.0	32.5	47.0
350,000 g/mol PMMA	70.5	31.9	48.1
520,000 g/mol PMMA	67.4	32.1	49.2
P3HT	92.9	54.7	32.3
SiO <sub>2</sub>	18.7	43.4	71.1

#### **Discussion:**

The data presented here documents and quantifies the impact of altering the processing conditions of spin coating immiscible polymer blends on the final film depth profile, including spin speed, polymer blend composition, and polymer molecular weight. Altering each of these parameters individually resulted in varying depth profiles and extent of stratification, yet the driving forces for these changes are less clear. Clearly, a number of factors may contribute to the stratification of a polymer blend during spin coating, including surface energy differences between two polymers, <sup>37</sup> the miscibility of the two polymers, the

relative solubility of each component in the pre-deposition solvent, the film formation time, and surface energy of the supporting substrate. It is clear that the surface energy differences between the two polymers does not fully explain our results, particularly the change in stratification with blend composition (Figure 2). To further investigate the importance of these driving forces of stratification, the Flory-Huggins interaction parameters,  $\chi$ , between PMMA, P3HT, and chlorobenzene were estimated using Equation 4.<sup>38</sup> The literature solubility parameters,  $\delta$ , for P3HT and PMMA are presented in Table 2 as well as the calculated  $\chi$  parameter between P3HT and PMMA ( $\chi = 1.08$ ) using Equation 4.

$$\chi = \frac{V_0}{RT} (\delta_a - \delta_b)^2$$
 Eq. (4)

A  $\chi$  parameter that is greater than 0.5 indicates poor polymer-polymer interactions, and an immiscible blend.<sup>39</sup> This is consistent with the results presented in Figure 2 that shows there is an increase of P3HT at the air interface with increase of P3HT loading in the blend, as this is consistent with increased phase separation between the two polymers and increased stratification as P3HT concentration in the blend increases, as shown in Figure 3. The increased immiscibility with increased P3HT concentration in the blend manifests as an increase in the P3HT concentration at the air interface. This result indicates that the immiscibility of P3HT and PMMA is a significant driving force for this stratification and that increasing the miscibility of two polymers will decrease the stratification.

**Table 2.** Solubility parameters at room temperature for P3HT and PMMA.

Material	δ (MPa <sup>1/2</sup> )	$\chi_{\text{P3HT-PMMA}}$
P3HT	$14.8^{40}$	1.08
PMMA	$19.5^{41}$	

The in-situ light reflectivity results (Figure 4) show that spin coating at 209.4 rad/s traps polymer movement over three times faster than the film formation process that occurs at the slowest spin speed of 52.4 rad/s. Since all other process conditions (blend composition, solvent interactions, blend molecular weight) are left unchanged, the kinetics of the film formation process are exclusively responsible for the disparity among all samples' final film depth profiles in Figure 5. Assuming the blend continually rearranges during the film formation process and is driven towards an equilibrium structure, the regulation

of film formation time provides insight into the progress towards equilibrium of each blend's thin film. For instance, a sample fabricated with a fast spin speed and shorter film formation time has a depth profile further from equilibrium than a sample processed with a slower spin speed and longer film formation time. The P3HT volume fraction depth profiles for the films formed from P3HT:131,500 g/mol dPMMA 20:80 blends (Figure 4) shows that P3HT segregates to the air surface (*Z*=0) for all three spin speeds with an increased P3HT concentration at the air interface with decreasing spin speed. Thus, the slower spin speed provides more time for the P3HT to be thermodynamically driven to the air interface, which is consistent with its lower surface energy. Figure 6 quantifies the percent stratification as a function of spin speed, where for each blend composition of P3HT and 131,500 g/mol dPMMA, the percent stratification increases with decreasing spin speed. This result indicates that the equilibrium of a P3HT:131,500 g/mol dPMMA blend is a more stratified sample with a P3HT dominated layer found at the air interface and a dPMMA rich layer found at the Si interface. Further, the effect of altering the P3HT:dPMMA blend composition is also evident at each examined spin speed (Figure 6), where increasing the P3HT concentration in the blend also increases the extent of stratification.

To broaden our understanding of the driving forces behind stratification of this system, PMMA molecular weights ranging from 20,000 g/mol – 520,000 g/mol were combined with P3HT in blend compositions of 5:95-20:80 and spin cast at 104.7 rad/s to investigate the effect of PMMA molecular weight on the film stratification patterns and extent of stratification. Altering the relative molecular weights of the two polymers in the blend allows us to evaluate the importance of entropic contributions to the stratification of the components in the film during the casting process. This is because smaller chains are entropically driven to the air interface to minimize the entropic penalty of confining a long polymer chain to an impenetrable interface. Figures 7 and 8 present the depth profiles and the extent of stratification of the cast films as a function of dPMMA molecular weight and P3HT:dPMMA blend composition, respectively. Figure 8 clearly shows that increasing the P3HT concentration in the blend, regardless of dPMMA molecular weight, increases the extent of stratification which is consistent with previously discussed results. The P3HT volume fraction depth profile for blends of 5:95 P3HT:dPMMA with varying dPMMA

molecular weight, as seen in Figure 7, shows various amounts of P3HT driven towards the air interface depending on the molecular weight of dPMMA. This result is quantified in Figure 7, where stratification decreases with decreasing dPMMA molecular weight, for all four blend compositions. This is consistent with P3HT and dPMMA of similar molecular weights having similar entropic driving forces. A reduction of the free energy of the system provides a driving force for the low molecular weight dPMMA to entropically segregate to the air interface, challenging the enthalpically driven sequestration of the P3HT at the air interface. This competition leads to less stratification due to the failure for P3HT and dPMMA to form independent pure layers.

All of the extent of stratification results are in good agreement with the calculated surface energies where the P3HT is primarily driven to the air interface and the decrease in dPMMA molecular weight results in a lower surface energy material, such that it is approaching the surface energy of P3HT. It is important to emphasize that the similarity of surface energy and entropic forces in the 20,000 g/mol dPMMA samples lead to less stratified films, while increasing the loading of P3HT in the blend still elicits an additional driving force for stratification. This result indicates that the entropic forces due to varying dPMMA molecular weight are not sufficient to overcome the immiscibility of the two polymers, P3HT and dPMMA.

These results clearly indicate that all processing conditions, not solely the miscibility of the polymer blend or their surface energies dictate and drive final film morphology, depth profiles, and extent of stratification. It is evident that by simply altering processing conditions, a targeted final film morphology may be fabricated without additional post-processing modifications. Although P3HT:dPMMA blends were studied here, the guidelines produced are based on the thermodynamic driving forces and kinetics of film formation during spin casting. Therefore, these results should provide guidelines to direct the stratification and assembly of a broad range of polymer blends. This foundation thus provides pathways to improve the structure and assembly of thin polymer blend films for a myriad of applications. These range from durable polymer coatings to organic electronic device processing where these results show that the interface

between the polymers can be controlled without extensive alteration to the thin film itself, as well as controllably altering the extent of stratification by changing the processing conditions.

#### **Conclusion:**

Neutron reflectivity experiments provide film depth profiles of various spin cast polymer blends processed by varying spin speed, blend composition, and polymer molecular weight. These results indicate that spin speed, blend composition, and molecular weight alter the stratification patterns of P3HT and dPMMA polymer blends and provide insight into the fundamental driving forces that guide the stratification process. In all cases, P3HT is driven toward the air interface and changing the processing conditions can further encourage this effect. This research also develops a method to analyze the degree of stratification, and therefore quantitatively compare the impact of processing parameters on the stratification process.

Our results show that the speed of spin casting controls film formation time where a slower spin speed leads to longer film formation. This longer film formation time allows the polymer layers more time to rearrange and approach equilibrium. By utilizing slower spin speeds, more stratified P3HT:dPMMA thin films emerge, when compared to samples formed at faster spinning speeds. In addition, altering the blend composition and molecular weight of the polymers also influence the final film depth profile. As the concentration of P3HT in the blend increases, the stratification of the blend increases due to the decrease in miscibility of the blend. Not only does the stratification increase, but increasing the amount of P3HT in the blend also elicits a sharpened interface between the two layers.

Incorporating lower molecular weight dPMMA into the blend alters the entropic driving forces in the stratification process, due to the increase in number of chain ends. This lower molecular weight dPMMA is entropically driven towards the air interface competing with P3HT, therefore decreasing stratification.

These results therefore provide guidelines to control and moderate the final film morphology and layering of deposited polymer blend thin films. Since P3HT and PMMA are widely used for organic field effect transistors, this research ultimately expands our ability to controllably alter the final film structure, and creates a pathway to better understand the correlation between processing conditions and thin film structure required for efficient device performance. Although this study outlines P3HT:dPMMA blends, the overall conclusions can be applied to other polymer blend systems and provides crucial insight that can

direct the development of optimal cost-efficient methods to fabricate multi-layer films with the desired structure without the need for post-modification processes.

#### **Acknowledgements:**

The authors gratefully acknowledge the National Science Foundation (DMR-1409034 and DMR-1808946) for support of this project. We acknowledge the support of the National Institute of Standards and Technology, U.S. Department of Commerce, in providing the neutron research facilities used in this work.

Certain commercial equipment, instruments, or materials (or suppliers, or software) are identified in this paper to foster understanding. Such identification does not imply recommendation or endorsement by the National Institute of Standards and Technology, nor does it imply that the materials or equipment identified are necessarily the best available for the purpose.

#### **Supporting Information:**

Eleven supporting figures, including volume fraction depth profiles, comparison of extent of stratification calculations for repeated samples, and an outlined example of extent of stratification calculation

#### **References:**

- (1) Liu, C.; Li, Y.; Lee, M. V; Kumatani, A.; Tsukagoshi, K. Self-Assembly of Semiconductor/insulator Interfaces in One-Step Spin-Coating: A Versatile Approach for Organic Field-Effect Transistors. *Phys. Chem. Chem. Phys.* **2013**, *15* (21), 7917–7933.
- (2) Grunwald, E.; Nuster, R.; Hammer, R.; Abmann, H.; Paltauf, G.; Brunner, R. Characterization of Polyimid-Multi-Layer Thin Films Combining Laser Ultrasonic Measurements and Numerical Evaluations. 2016 17th Int. Conf. Therm. Mech. Multi-Physics Simul. Exp. Microelectron. Microsystems, EuroSimE 2016 2016, No. Mcl, 1–5.
- (3) Ulaeto, S. B.; Rajan, R.; Pancrecious, J. K.; Rajan, T. P. D.; Pai, B. C. Developments in Smart Anticorrosive Coatings with Multifunctional Characteristics. *Prog. Org. Coatings* **2017**, *111* (December 2016), 294–314.
- (4) Ahmadi Lakalayeh, G.; Rahvar, M.; Haririan, E.; Karimi, R.; Ghanbari, H. Comparative Study of Different Polymeric Coatings for the next-Generation Magnesium-Based Biodegradable Stents. *Artif. Cells, Nanomedicine Biotechnol.* **2017**, *46*, 1–10.
- (5) Cristea, M. V.; Riedl, B.; Blanchet, P. Effect of Addition of Nanosized UV Absorbers on the Physico-Mechanical and Thermal Properties of an Exterior Waterborne Stain for Wood. *Prog. Org. Coatings* **2011**, *72* (4), 755–762.
- (6) Hennessy, M. G.; Burlakov, V. M.; Münch, A.; Wagner, B.; Goriely, A. Propagating Topological

- Transformations in Thin Immiscible Bilayer Films. Epl 2014, 105 (6).
- (7) Beaugendre, A.; Degoutin, S.; Bellayer, S.; Pierlot, C.; Duquesne, S.; Casetta, M.; Jimenez, M. Progress in Organic Coatings Self-Stratifying Coatings: A Review. *Prog. Org. Coatings* **2017**, *110*, 210–241.
- (8) Schaefer, C.; Michels, J. J.; Van Der Schoot, P. Dynamic Surface Enrichment in Drying Thin-Film Binary Polymer Solutions. *Macromolecules* **2017**, *50* (15), 5914–5919.
- (9) Gruner, G. Carbon Nanotube Films for Transparent and Plastic Electronics. *J. Mater. Chem.* **2006**, *16* (35), 3533.
- (10) Qiu, L.; Lim, J. A.; Wang, X.; Lee, W. H.; Hwang, M.; Cho, K. Versatile Use of Vertical-Phase-Separation-Induced Bilayer Structures in Organic Thin-Film Transistors. *Adv. Mater.* **2008**, *20* (6), 1141–1145.
- (11) Wang, X.; Lee, W. H.; Zhang, G.; Wang, X.; Kang, B.; Lu, H.; Qiu, L.; Cho, K. Self-Stratified Semiconductor/dielectric Polymer Blends: Vertical Phase Separation for Facile Fabrication of Organic Transistors. *J. Mater. Chem. C* **2013**, *I* (25), 3989.
- (12) Kline, R. J.; McGehee, M. D.; Kadnikova, E. N.; Liu, J.; Fréchet, J. M. J.; Toney, M. F. Dependence of Regioregular poly(3-Hexylthiophene) Film Morphology and Field-Effect Mobility on Molecular Weight. *Macromolecules* **2005**, *38* (8), 3312–3319.
- (13) Paterson, A. F.; Lin, Y.-H.; Mottram, A. D.; Fei, Z.; Niazi, M. R.; Kirmani, A. R.; Amassian, A.; Solomeshch, O.; Tessler, N.; Heeney, M.; et al. The Impact of Molecular P-Doping on Charge Transport in High-Mobility Small-Molecule/Polymer Blend Organic Transistors. *Adv. Electron. Mater.* **2017**, *1700464*, 1700464.
- (14) Guo, P.; Luo, G.; Su, Q.; Li, J.; Zhang, P.; Tong, J.; Yang, C.; Xia, Y.; Wu, H. Boosting Up Performance of Inverted Photovoltaic Cells from Bis(alkylthien-2-yl)dithieno[2,3-d:2',3'-d']benzo[1,2-b:4',5'-B']di Thiophene-Based Copolymers by Advantageous Vertical Phase Separation. *ACS Appl. Mater. Interfaces* **2017**, *9* (12), 10937–10945.
- (15) Chen, L. M.; Hong, Z.; Li, G.; Yang, Y. Recent Progress in Polymer Solar Cells: Manipulation of Polymer: Fullerene Morphology and the Formation of Efficient Inverted Polymer Solar Cells. *Adv. Mater.* **2009**, *21* (14–15), 1434–1449.
- (16) Alcazar, D.; Wang, F.; Swager, T. M.; Thomas, E. L. Gel Processing for Highly Oriented Conjugated Polymer Films Gel Processing for Highly Oriented Conjugated Polymer Films. **2008**, 9863–9868.
- (17) Barbero, D. R.; Steiner, U. Nonequilibrium Polymer Rheology in Spin-Cast Films. *Phys. Rev. Lett.* **2009**, *102* (24), 1–4.
- (18) Heriot, S. Y.; Jones, R. a L. An Interfacial Instability in a Transient Wetting Layer Leads to Lateral Phase Separation in Thin Spin-Cast Polymer-Blend Films. *Nat. Mater.* **2005**, *4* (10), 782–786.
- (19) Xu, Z.; Chen, L. M.; Yang, G.; Huang, C. H.; Hou, J.; Wu, Y.; Li, G.; Hsu, C. S.; Yang, Y. Vertical Phase Separation in poly(3-Hexylthiophene): Fullerene Derivative Blends and Its Advantage for Inverted Structure Solar Cells. *Adv. Funct. Mater.* **2009**, *19* (8), 1227–1234.
- (20) Yan, Y.; Liu, X.; Wang, T. Conjugated-Polymer Blends for Organic Photovoltaics: Rational Control of Vertical Stratification for High Performance. *Adv. Mater.* **2017**, No. February.
- (21) Ge, F.; Liu, Z.; Lee, S. B.; Wang, X.; Zhang, G.; Lu, H.; Cho, K.; Qiu, L. Bar-Coated Ultrathin Semiconductor from Polymer Blend for One-Step Organic Field-Effect Transistors. *ACS Appl. Mater. Interfaces* **2018**, *10*, 21510–21517.

- (22) Zhang, L.; Yang, D.; Wang, Y.; Wang, H.; Song, T.; Fu, C. Performance Enhancement of FET-Based Photodetector by Blending P3HT With PMMA. **2015**, *27* (14), 1535–1538.
- (23) Wu, M. C.; Liao, H. C.; Chou, Y.; Hsu, C. P.; Yen, W. C.; Chuang, C. M.; Lin, Y. Y.; Chen, C. W.; Chen, Y. F.; Su, W. F. Manipulation of Nanoscale Phase Separation and Optical Properties of P3HT/PMMA Polymer Blends for Photoluminescent Electron Beam Resist. *J. Phys. Chem. B* **2010**, *114* (32), 10277–10284.
- Gburek, B.; Wagner, V. Influence of the Semiconductor Thickness on the Charge Carrier Mobility in P3HT Organic Field-Effect Transistors in Top-Gate Architecture on Flexible Substrates. *Org. Electron. physics, Mater. Appl.* **2010**, *11* (5), 814–819.
- (25) Sirringhaus, H. Device Physics of Solution-Processed Organic Field-Effect Transistors. *Adv. Mater.* **2005**, *17* (20), 2411–2425.
- (26) Herlogsson, L.; Noh, Y. Y.; Zhao, N.; Crispin, X.; Sirringhaus, H.; Berggren, M. Downscaling of Organic Field-Effect Transistors with a Polyelectrolyte Gate Insulator. *Adv. Mater.* **2008**, *20* (24), 4708–4713.
- (27) Kergoat, L.; Battaglini, N.; Miozzo, L.; Piro, B.; Pham, M. C.; Yassar, A.; Horowitz, G. Use of poly(3-Hexylthiophene)/poly(methyl Methacrylate) (P3HT/PMMA) Blends to Improve the Performance of Water-Gated Organic Field-Effect Transistors. *Org. Electron. physics, Mater. Appl.* **2011**, *12* (7), 1253–1257.
- (28) Toolan, D. T. W.; Isakova, A.; Hodgkinson, R.; Reeves-Mclaren, N.; Hammond, O. S.; Edler, K. J.; Briscoe, W. H.; Arnold, T.; Gough, T.; Topham, P. D.; et al. Insights into the Influence of Solvent Polarity on the Crystallization of Poly(ethylene Oxide) Spin-Coated Thin Films via in Situ Grazing Incidence Wide-Angle X-Ray Scattering. *Macromolecules* **2016**, *49* (12), 4579–4586.
- (29) Ohmori, M.; Nakatani, M.; Kajii, H.; Miyamoto, A.; Yoneya, M.; Fujii, A.; Ozaki, M. Fabrication of Field-Effect Transistor Utilizing Oriented Thin Film of Octahexyl-Substituted Phthalocyanine and Its Electrical Anisotropy Based on Columnar Structure. *Jpn. J. Appl. Phys.* **2018**, *57* (3).
- (30) Zhao, K.; Wodo, O.; Ren, D.; Khan, H. U.; Niazi, M. R.; Hu, H.; Abdelsamie, M.; Li, R.; Li, E. Q.; Yu, L.; et al. Vertical Phase Separation in Small Molecule:Polymer Blend Organic Thin Film Transistors Can Be Dynamically Controlled. Adv. Funct. Mater. 2016, 26 (11), 1737–1746.
- (31) Emerson, J. A.; Garabedian, N. T.; Moore, A. C.; Burris, D. L.; Furst, E. M.; Epps, T. H. Unexpected Tribological Synergy in Polymer Blend Coatings: Leveraging Phase Separation to Isolate Domain Size Effects and Reduce Friction. *ACS Appl. Mater. Interfaces* **2017**, *9* (39), 34480–34488.
- (32) Kienzle, P. A.; O'Donovan, K. V.; Ankner, J. F.; Berk, N. F.; Majkrzak, C. F. http://www.ncnr.nist.gov/reflpak http://www.ncnr.nist.gov/reflpak.
- (33) Nelson, A. Co-Refinement of Multiple-Contrast neutron/X-Ray Reflectivity Data Using MOTOFIT. *J. Appl. Crystallogr.* **2006**, *39* (2), 273–276.
- (34) Balzarotti, R.; Cristiani, C.; Francis, L. F. Spin Coating Deposition on Complex Geometry Substrates: Influence of Operative Parameters. *Surf. Coatings Technol.* **2017**, *330* (August), 1–9.
- (35) Brigham, N.; Nardi, C.; Carandang, A.; Allen, K.; Van Horn, R. M. Manipulation of Crystallization Sequence in PEO-B-PCL Films Using Solvent Interactions. *Macromolecules* **2017**, *50* (22), 8996–9007.
- (36) Owens, D. K.; Wendt, R. C. Estimation of the Surface Free Energy of Polymers. *J. Appl. Polym. Sci.* **1969**, *13* (8), 1741–1747.
- (37) Campoy-Quiles, M.; Ferenczi, T.; Agostinelli, T.; Etchegoin, P. G.; Kim, Y.; Anthopoulos, T. D.;

- Stavrinou, P. N.; Bradley, D. D. C.; Nelson, J. Morphology Evolution via Self-Organization and Lateral and Vertical Diffusion in Polymer:fullerene Solar Cell Blends. *Nat. Mater.* **2008**, *7* (2), 158–164.
- (38) Rubinstein, M.; Colby, R. H. Polymer Physics; Oxford University Press, 2003.
- (39) Hiemenz, P. C.; Lodge, T. P. *Polymer Chemistry*, Second Edi.; Taylor & Francis Group, LLC: Boca Raton, FL, 2007.
- (40) Emerson, J. A.; Toolan, D. T. W.; Howse, J. R.; Furst, E. M.; Epps, T. H. Determination of Solvent Polymer and Polymer Polymer Flory Huggins Interaction Parameters for Poly(3-Hexylthiophene) via Solvent Vapor Swelling. *Macrolecules* **2013**.
- (41) Lindvig, T.; Michelsen, M. L.; Kontogeorgis, G. M. A Flory-Huggins Model Based on the Hansen Solubility Parameters. *Fluid Phase Equilib.* **2002**, *203* (1–2), 247–260.
- (42) Zhang, R.; Lee, B.; Stafford, C. M.; Douglas, J. F.; Dobrynin, A. V.; Bockstaller, M. R.; Karim, A. Entropy-Driven Segregation of Polymer-Grafted Nanoparticles under Confinement. *Proc. Natl. Acad. Sci.* 2017, 114 (10), 2462–2467.
- (43) Zhu, G.; Huang, Z.; Xu, Z.; Yan, L. T. Tailoring Interfacial Nanoparticle Organization through Entropy. *Acc. Chem. Res.* **2018**, *51* (4), 900–909.

### For Table of Contents use only:

# Elucidating the Kinetic and Thermodynamic Driving Forces in Polymer Blend Film Self-Stratification

Samantha J. Rinehart<sup>1</sup>, Guangcui Yuan<sup>2,3</sup>, and \*Mark D. Dadmun<sup>1,4</sup>

